JOURNAL OF VIROLOGY, Nov. 2002, p. 11065–11078 Vol. 76, No. 21
0022-538X/02/$04.00+0 DOI: 10.1128/JVI.76.21.11065–11078.2002

Systematic Assembly of a Full-Length Infectious cDNA of Mouse Hepatitis Virus Strain A59

Boyd Yount,[1] Mark R. Denison,[2] Susan R. Weiss,[3] and Ralph S. Baric[1,4]*

Department of Epidemiology, School of Public Health, University of North Carolina at Chapel Hill, Chapel Hill, North Carolina 27599-7435[1]; Department of Pediatrics and Microbiology and Immunology, Elizabeth B. Lamb Center for Pediatric Research, Vanderbilt University Medical Center, Nashville, Tennessee 37232-2581[2]; Department of Microbiology, School of Medicine, University of Pennsylvania, Philadelphia, Pennsylvania 19104-6076[3]; and Department of Microbiology and Immunology, School of Medicine, University of North Carolina at Chapel Hill, Chapel Hill, North Carolina 27599-7290[4]

Received 31 January 2002/Accepted 22 July 2002

A novel method was developed to assemble a full-length infectious cDNA of the group II coronavirus mouse hepatitis virus strain A59 (MHV-A59). Seven contiguous cDNA clones that spanned the 31.5-kb MHV genome were isolated. The ends of the cDNAs were engineered with unique junctions and assembled with only the adjacent cDNA subclones, resulting in an intact MHV-A59 cDNA construct of ~31.5 kb in length. The interconnecting restriction site junctions that are located at the ends of each cDNA are systematically removed during the assembly of the complete full-length cDNA product, allowing reassembly without the introduction of nucleotide changes. RNA transcripts derived from the full-length MHV-A59 construct were infectious, although transfection frequencies were enhanced 10- to 15-fold in the presence of transcripts encoding the nucleocapsid protein N. Plaque-purified virus derived from the infectious construct replicated efficiently and displayed similar growth kinetics, plaque morphology, and cytopathology in murine cells as did wild-type MHV-A59. Molecularly cloned viruses recognized the MHV receptor (MHVR) for docking and entry, and pretreatment of cells with monoclonal antibodies against MHVR blocked virus entry and replication. Cells infected with molecularly cloned MHV-A59 virus expressed replicase (gene 1) proteins identical to those of laboratory MHV-A59. Importantly, the molecularly cloned viruses contained three marker mutations that had been derived from the engineered component clones. Full-length infectious constructs of MHV-A59 will permit genetic modifications of the entire coronavirus genome, particularly in the replicase gene. The method has the potential to be used to construct viral, microbial, or eukaryotic genomes approaching several million base pairs in length and used to insert restriction sites at any given nucleotide in a microbial genome.

The Nidovirales order includes mammalian and avian positive-polarity, single-stranded RNA viruses in the arterivirus and coronavirus families (43). The *Coronaviridae* family is further subdivided into the *Coronavirus* and *Torovirus* genera (14, 45). Despite remarkable size differences in the genomic RNA (13 to 32 kb), the polycistronic genome organization and regulation of gene expression from a nested set of subgenomic mRNAs are similar for all members of the order (29, 45). Coronaviruses contain the largest single-stranded, plus-polarity RNA genome in nature, ranging in size from about 27 to 31 kb in length, and are divided into three subgroups based upon antigenic and sequence comparisons (29, 43). The group I coronaviruses include human coronavirus strain 229E (HCV 229E) and transmissible gastroenteritis virus (TGEV). The group II coronaviruses contain mouse hepatitis virus (MHV), bovine coronavirus, and HCV OC43. Bovine coronavirus is an important pathogen of cattle while HCV infection is associated with a significant percentage of common colds in winter. The group III coronaviruses contain infectious bronchitis virus (IBV).

* Corresponding author. Mailing address: Department of Epidemiology, School of Public Health, McGaveran-Greenberg Hall, CB 7435, University of North Carolina at Chapel Hill, Chapel Hill, NC 27599-7435. Phone: (919) 966-3895. Fax: (919) 966-2089. E-mail: rbaric@sph.unc.edu.

The MHV-A59 and MHV-JHM strains are the most extensively studied group II coronaviruses, and infection in susceptible mice results in a panencephalitis with acute and chronic demyelination that is histologically similar to multiple sclerosis in humans (28). MHV-A59 is also hepatotropic, and infection results in hepatitis (30). The MHV-A59 virion contains a ~31.5-kb genome that encodes ~10 large open reading frames (ORFs) (8). The genomic RNA is packaged by a 50-kDa nucleocapsid protein (N) into a helical nucleocapsid structure and acquires an envelope by budding into intermediate compartments between the endoplasmic reticulum and the Golgi complex (18, 37, 38, 50). The MHV virion contains three or four virus proteins including a spike glycoprotein of ~180/90 kDa (S), a 65-kDa hemagglutinin esterase (HE), a 23-kDa membrane glycoprotein (M), and an ~11-kDa E protein (33, 34, 53). Note that the HE glycoprotein is encoded as a pseudogene in some MHV strains, including MHV-A59 (34, 51). Consequently, its function in MHV replication and pathogenesis is not clear. Much of our knowledge concerning the replication strategy of coronaviruses has focused on the use of MHV as a model for pathogenesis, docking and entry, receptor usage, transcription, replication, polymerase function, and assembly and release (4, 5, 6, 9, 10, 12, 15, 21, 22, 23, 40, 41, 42, 54).

The MHV-A59 gene 1 (replicase gene) is about 22 kb in

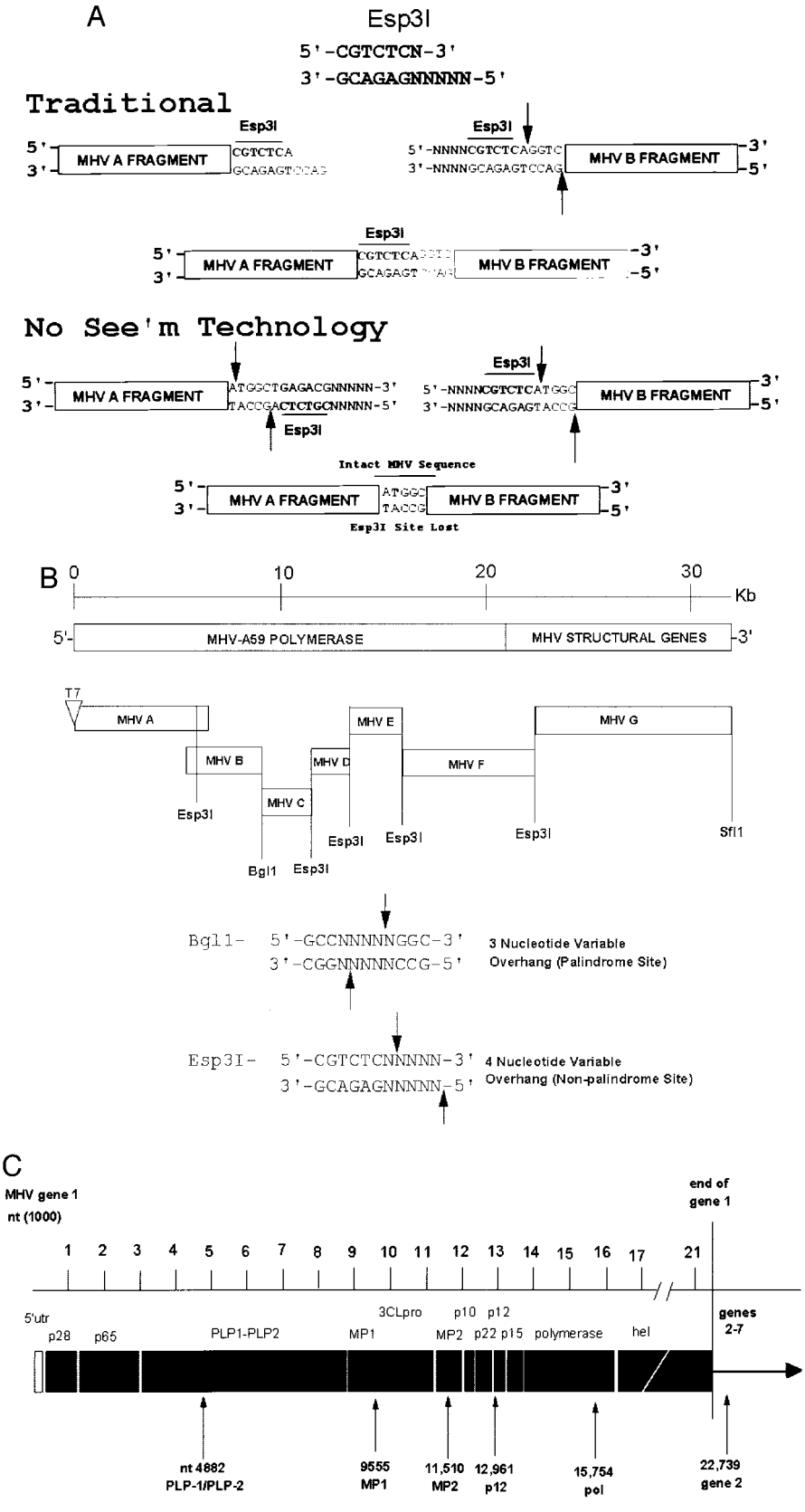
A
Esp3I
5'-CGTCTCN-3'
3'-GCAGAGNNNNN-5'
Traditional
Esp3I
MHV A FRAGMENT
MHV B FRAGMENT
No See'm Technology
Intact MHV Sequence
Esp3I Site Lost
B
0
10
20
30
Kb
MHV-A59 POLYMERASE
MHV STRUCTURAL GENES
T7
MHV A
MHV B
MHV C
MHV D
MHV E
MHV F
MHV G
Esp3I
Bgl1
Sfi1
Bgl1- 5'-GCCNNNNNGGC-3'
3'-CGGNNNNNCCG-5'
3 Nucleotide Variable
Overhang (Palindrome Site)
Esp3I- 5'-CGTCTCNNNNN-3'
3'-GCAGAGNNNNN-5'
4 Nucleotide Variable
Overhang (Non-palindrome Site)
C
MHV gene 1
nt (1000)
end of
gene 1
1 2 3 4 5 6 7 8 9 10 11 12 13 14 15 16 17 21
5'utr
p28
p65
PLP1-PLP2
3CLpro
MP1
p10
p12
MP2
p22
p15
polymerase
hel
genes
2-7
nt 4882
PLP-1/PLP-2
9555
MP1
11,510
MP2
12,961
p12
15,754
pol
22,739
gene 2

length and contains two large overlapping ORFs (1a and 1b) with 1b in the −1 reading frame with respect to ORF1a (8, 12). ORF1b expression requires a ribosomal frameshift at a pseudoknot structure in the 1a-1b overlap region (12). Thus, the replicase gene is capable of expressing two large polyproteins, the ORF1a polyprotein (pp1a, 495 kDa) and the 1a/ab fusion polyprotein (pp1ab, 803 kDa) (8, 12, 25). ORF1a encodes at least three experimentally confirmed protease activities including two papain-like proteases (PLP1 and PLP2) and a polio 3C-like protease (3CLpro) (9, 20, 31, 32,). Neither pp1a nor pp1ab is detected intact in MHV-infected cells since the proteinases process the polyproteins cotranslationally and posttranslationally into at least 14 mature replicase proteins (9, 10, 19, 20, 31, 32). The PLP1 cleavage products include the p28 and p65 proteins, both of which are derived from the N terminus of ORF1a (20). The 3CLpro cleavage products include MP1, 3CLpro, αp10, αp22, αp12, and αp15, all of which are derived from the C terminus of pp1a (10). ORF1b is cleaved by 3CLpro into at least four mature products, including putative polymerase and helicase polypeptides (19). The functions of most of the replicase proteins in MHV-A59 replication and pathogenesis are unknown, although genetic complementation analysis with temperature-sensitive mutations suggests at least eight distinct functions that influence RNA synthesis (46). Many of the replicase proteins are associated with membranes that are also sites of viral RNA synthesis (19, 44).

Molecular genetic analysis of the structure and function of RNA virus genomes has been profoundly advanced by the availability of full-length cDNA clones, from which infectious RNA transcripts can be derived that replicate efficiently when introduced into permissive cell lines (1, 2, 11). Until recently, the large size of the coronavirus RNA genome, coupled with regions of chromosomal instability, hindered the development of full-length infectious cDNAs. To circumvent these problems, a novel targeted recombination-based approach was developed, which involved the use of a molecularly cloned defective-interfering-like RNA and took advantage of high RNA recombination frequencies during mixed MHV infection (26, 27, 35). Targeted recombination has been very useful for studies of the 3′-most ~9 kb of the MHV genome but has not been used for other regions of the genome, notably the replicase gene (26, 27).

Two general strategies have recently been developed to assemble full-length infectious cDNAs of coronavirus RNA genomes. One strategy involved the stable cloning of full-length group I coronaviruses (TGEV and HCV 229E) cDNAs into bacterial artificial chromosomes or vaccinia virus (3, 48). Then, molecularly cloned recombinant virus was recovered following either a DNA- or an RNA-based launch, respectively. A full-length infectious cDNA of IBV has also been assembled in vaccinia virus vectors (13). In contrast to these approaches, we have assembled a full-length infectious cDNA of TGEV by in vitro ligation from six component subclones and the subsequent in vitro transcription of infectious RNAs (52). In this system, each of the component clones terminates in a restriction site that leaves a variable 3- or 4-nucleotide end, generated by a *Bgl*I or *Bst*XI site, respectively. The different ends target assembly with only the appropriate adjacent subclones. A strength of this system is that reverse genetic applications are simplified in the component clones compared with the sequence complexity of full-length cDNAs. This allows for rapid reverse genetic applications within individual segments of the viral genome as well as the ability to rapidly mix and match mutations in different regions of the genome (17, 52).

In this study we describe a full-length cDNA of MHV-A59, the first group II coronavirus that has been successfully recovered from a genome-length reverse genetic system. The assembly of full-length cDNAs of the group II coronaviruses has been hampered by the presence of numerous toxic regions in the viral ORF1 polymerase, which are unstable in bacteria with high- or low-copy-number plasmid vectors. We have solved this problem by using a strategy that separates the toxic regions during cloning and then regenerates the exact wild-type MHV sequence at the junctions between the component clones. This vector will allow for detailed reverse genetic applications throughout the entire MHV genome and will serve as a model for the assembly of other group II coronavirus full-length cDNAs, as well as other RNA and DNA viruses and microbial genomes.

MATERIALS AND METHODS

Cells and viruses. Delayed brain tumor (DBT) cells were originally established from a CDF1 mouse inoculated intracerebrally with the Schmidt-Ruppin strain of Rous sarcoma virus. DBT cells were maintained in Eagle's minimum essential medium supplemented with 10% fetal clone II, 5% tryptose phosphate broth, 0.05 μg of gentamicin/ml, and 0.25 μg of kanamycin/ml. DBT-9 cells were

FIG. 1. Strategy to assemble an infectious cDNA of MHV-A59. (A) *Esp*3I cloning properties. In the traditional mode, an *Esp*3I site resides at the 3′ end of the MHV A subclone and upon cleavage results in a novel 4-nucleotide overhang which will specifically anneal with the complementary 4-nucleotide overhang generated by an identical *Esp*3I site located at the 5′ end of the MHV B fragment. Note that the MHV wild-type sequence is re-formed intact and the *Esp*3I site is retained in the virus sequence. However, the *Esp*3I recognition site is a nonpalindromic sequence, and as such, a simple flip in orientation allows for the specific removal of the *Esp*3I recognition site in the MHV A and B subclones, leaving 4-nucleotide complementary overhangs, which re-form the intact wild-type sequence upon ligation. No evidence of the *Esp*3I site that has been engineered into the component clones should remain in the assembled product (No See'm technology). In this cartoon, the sequences represent wild-type MHV sequence but are not the exact nucleotides encoded at the MHV A/B junction (Tables 1 and 2). (B) Component clones used in the assembly of a full-length MHV-A59 cDNA. The MHV genome is a linear positive-polarity RNA of about 31,500 nucleotides in length. By using RT-PCR and unique oligonucleotide primer mutagenesis, seven clones spanning the entire MHV genome were isolated by standard recombinant DNA techniques. Unique *Esp*3I and *Bgl*I sites, located at the junctions between each of the cDNA clones, were used to assemble a full-length infectious cDNA. A unique T7 start site was inserted at the 5′ end of clone A, and a 25-nucleotide T tail and downstream *Sfi*I site were encoded at the 3′ end of clone G. The approximate location of each site is shown. (C) Location of the MHV component clone junctions. MHV ORF1a and ORF1b polyproteins are proteolytically processed into numerous smaller proteins, which presumably function to direct virus replication and transcription. The component clone A/B, B/C, C/D, D/E, and E/F junctions are shown relative to the ORF1 polyproteins synthesized during MHV-A59 infection. The F/G junction resides in the HE glycoprotein pseudogene. utr, untranslated region; nt, nucleotide.

TABLE 1. Design of the MHV-A59 junction sequences[a]

MHV-A59 subclone	Restriction site junction	Location	Junction
A	5′←TCGTTAA↓CAAATGAGACGNNNN-3′ 3′←AGCAATTGTTT↑**ACTCTGC**NNNN-5′	3′-end A fragment, *Esp*3I, nt 4882	A/B
B	5′-NNNN**CGTCTC**A↓CAAATTTGAT→3′ 3′-NNNNGCAGAGTGTTT↑AAACTA→5′	5′-end B fragment, *Esp*3I, nt 4883	A/B
	5′←CTTT**GCCT**↓**TAACGGC**GAGTTC-3′ 3′←GAAA**CGGAATT**↑**GCCG**CTCAAG-5′	3′-end B fragment, *Bgl*I, nt 9555	B/C
C	5′-CTTT**GCCT**↓**TAACGGC**GAGTTC→3′ 3′-GAAA**CGGAATT**↑**GCCG**CTCAAG→5′	5′-end C fragment, *Bgl*I, nt 9556	B/C
	5′←TAGCATA↓AACCAGAGACGNNNN-3′ 3′←ATCGTATTTGG↑T**CTCTGC**NNNN-5′	3′-end C fragment, *Esp*3I, nt 11510	C/D
D	5′-NNNN**CGTCTC**A↓AACCACGACGTC→3′ 3′-NNNNGCAGAGTTTGG↑TGCTGCAG→5′	5′-end D fragment, *Esp*3I, nt 11511	C/D
	5′←TATGCTAT↓CCTAAGAGACGNNNN-3′ 3′←ATACGATAGGAT↑T**CTCTGC**NNNN-5′	3′-end D fragment, *Esp*3I, nt 12961	D/E
E	5′-NNNN**CGTCTC**T↓CCTAAGTGACTG→3′ 3′-NNNNGCAGAGAGGAT↑TCACTGAC→5′	5′-end E fragment, *Esp*3I, nt 12962	D/E
	5′←ACTCTAAT↓GTCTAGAGACGNNNN-3′ 3′←TGAGATTACAGA↑T**CTCTGC**NNNN-5′	3′-end E fragment, *Esp*3I, nt 15754	E/F
F	5′-NNNN**CGTCTC**T↓GTCTATCGTGCG→3′ 3′-NNNNGCAGAGACAGA↑TAGCACGC→5′	5′-end F fragment, *Esp*3I, nt 15755	E/F
	5′←ACAGTCGG↓TCCGAGAGACGNNNN-3′ 3′←GTCAGCCAGGC↑T**CTCTGC**NNNN-5′	3′-end F fragment, *Esp*3I, nt 22739	F/G
G	5′-NNNN**CGTCTC**G↓TCCGACTGTACC→3′ 3′-NNNNGCAGAGCAGGC↑TGACATGG→5′	5′-end G fragment, *Esp*3I, nt 22740	F/G

[a] Horizontal arrows indicate the direction of the MHV coding sequences in an individual clone, vertical arrows indicate the site of restriction, and an underline represents the resulting 3- or 4-nucleotide overhang generated at each junction. Various restriction sites are shown in boldface. N, any nucleotide can be inserted at this position. The 3′ end of MHV G is as described for pMH54 (27). nt, nucleotide.

isolated from DBT cells by fluorescence-activated cell sorting with a monoclonal antibody directed against the MHV receptor (MHVR) (15, 23). Consequently, these cells express a relatively uniform and abundant amount of MHVR, the receptor for MHV-A59 docking and entry into cells (15, 16). Baby hamster kidney (BHK) cells were kindly provided by Robert E. Johnston (University of North Carolina at Chapel Hill) and maintained in alpha minimum essential medium supplemented with 10% fetal calf serum, 10% tryptose phosphate broth, 0.05 μg of gentamicin/ml, and 0.25 μg of kanamycin/ml. Plasmid encoding the MHVR (Bgp1a) and monoclonal antibodies against the murine MHVR were kindly provided by K. Holmes, University of Colorado Health Sciences Center. BHK cells transfected with the MHVR were subjected to fluorescence-activated cell sorting twice with monoclonal antibody CC1 and maintained in alpha minimum essential medium containing 10% fetal calf serum, 10% tryptose phosphate broth, 0.05 μg of gentamicin/ml, 0.25 μg of kanamycin/ml, and 800 μg of Geneticin (G418 sulfate; Sigma)/ml.

The MHV-A59 strain of MHV was used throughout the course of these experiments. Our wild-type MHV-A59 was obtained from Larry Sturman and had been plaque purified three times through L2 cells maintained at 40°C. MHV-A59 and molecularly cloned viruses were plaque purified in DBT cells, and stocks were grown in DBT cells.

Blockade experiments. DBT or BHK-MHVR cells were seeded at densities of 2×10^5 into four-chambered LabTek slides overnight and then incubated with 100 μl of a 1:4 dilution of anti-MHVR monoclonal antibody CC1 for 45 min at room temperature. The CC1 monoclonal antibody was collected from hybridoma culture supernatants and binds to the N-terminal domain of MHVR (23). After incubation, the antibodies were removed and the cells were challenged with MHV-A59 or molecularly cloned viruses at a multiplicity of infection (MOI) of 10 for 1 h at room temperature. The virus inoculates were then removed, the cultures were washed twice with phosphate-buffered saline (PBS) to remove residual virus, and 750 μl of complete medium containing a 1:16 dilution of CC1 was added to the cultures. Virus samples were harvested at different times postinfection and stored at −70°C for plaque assay in DBT-9 cells (15).

Mutagenesis, cloning, and sequencing of the MHV-A59 genome. The cloning strategy for a full-length MHV-A59 construct is illustrated in Fig. 1 and is based upon the observation that the *Esp*3I restriction endonuclease cleaves at a specific nonpalindromic sequence and leaves highly variable 4-nucleotide ends that will not randomly self-assemble. Rather, these DNAs will anneal only with fragments containing the complementary 4-nucleotide overhang generated at identical *Esp*3I sites. The MHV-A59 genome was cloned from infected DBT cell intracellular RNA by reverse transcription-PCR (RT-PCR) with primer pairs directed against conserved regions in MHV-A59 and MHV-JHM (Tables 1 and 2). To create unique junction sites for assembly of a full-length MHV-A59 cDNA construct, primer-mediated PCR mutagenesis was used to insert unique *Esp*3I restriction sites at the 5′ and 3′ ends of each subclone (Table 2) (Fig. 1). These primer pairs did not alter the coding sequence and resulted in RT-PCR amplicons ranging in size from ~1.4 to 8.6 kb in length. Briefly, total intracellular RNA was isolated from MHV-A59-infected cells with Trizol reagent according to the manufacturer's directions (Invitrogen). To isolate the MHV-A59 subclones, reverse transcription was performed with Superscript II and oligodeoxynucleotide primers according to the manufacturer's recommendations (Gibco BRL). For sequence comparisons and primer design, we used the MHV-A59 sequence as reported in GenBank (30). Following cDNA synthesis at 50°C for 1 h, the cDNA was denatured for 2 min at 94°C and amplified by PCR with Expand Long TAQ polymerase (Boehringer Mannheim Biochemical) for 25 cycles of 94°C for 30 s, 58°C for 25 to 30 s, and 68°C for 1 to 7 min depending upon the size of the amplicon. The PCR amplicons were isolated from agarose gels and cloned into Topo II TA (Invitrogen), pGem-TA cloning (Promega), or pSMART (Lucigen) vectors according to the manufacturer's directions.

Three to seven independent clones of each MHV-A59 amplicon were isolated and sequenced by using a panel of insert-specific primers and an ABI model automated sequencer. A consensus sequence for each of the cloned fragments was determined, and a consensus clone was assembled by using restriction enzymes and standard recombinant DNA techniques.

Assembly of a full-length MHV-A59 infectious construct (icMHV-A59). Each of the plasmids was grown to a high concentration, isolated, and digested, or double digested, with *Esp*3I, *Bgl*I, or *Not*I according to the manufacturer's directions (New England Biolabs) (Fig. 1A). The MHV-A59 A clone was digested with *Mlu*I, which is located in the Topo II plasmid, treated with calf intestine alkaline phosphatase, and subsequently digested with *Esp*3I. The MHV-A59 G clone was *Sfi*I digested, treated with calf alkaline phosphatase, and then *Esp*3I digested. All other vectors were digested with *Esp*3I or *Esp*3I/*Bgl*I. The appropriately sized cDNA inserts were visualized in 0.8 to 1.2% agarose gels in TAE buffer (Tris-acetate-EDTA) with Darkreader technology (Claire Chemical Research, Denver, Colo.) and isolated with Qiaex II gel extraction kits (Qiagen Inc., Valencia, Calif.). Darkreader technology allows DNA visualization under visible light and does not cause DNA damage. Appropriate cDNA subsets (A+B, C+D+E, and F+G) were pooled into 100- to 200-μl aliquots, and equivalent amounts of each DNA were ligated with T4 DNA ligase (15 U/100 μl) at 16°C

TABLE 2. Primer pairs used in cloning the individual MHV-A59 amplicons

Primer designation	Nucleotide sequence[a]	Genome location	Orientation	Purpose
MHV A 5′ 17(+)	5′- **NGTTTAAAC**NNNNNNTAATACGACTCACTATAGATAAGAGTGATTGGCGTCCG-3′ (*Pme*I)	1–21	+	T7 start
MHV A 3520-mu(+)	5′- TAAAGTGGGTTTCATCACTCGGCAC-3′ (C C)	3528–3506	−	Overlapping PCR *Esp*3I mutagenesis
MHV A 3520-mu(−)	5′- GCCGAGTGATGAAACCCACTTTAAAGTG-3′ (G G)	3506–3533	+	Overlapping PCR *Esp*3I mutagenesis
MHV A 4870(−)	5′- **CGTCTC**ATTTGTTAACCAGTCGCCAGTCTGTGGGCAG-3′ (*Esp*3I; G A)	4887–4856	−	MHV A/B junction
MHV B 4870(+)	5′- **CGTCTC**ACAAATTTGATAGTGTTGATGGTG-3′	4888–4905	+	MHV A/B junction
MHV B 9620(−)	5′- ACTGAACTCGCCGTTAAGGC-3′	9571–9552	−	MHV B/C junction
MHV C 8933(+)	5′- GGTATAGTCTACATTTGGTC-3′ (T)	8932–8952	+	MHV B/C junction
MHV C 11511(−)	5′- **CGTCTC**TGGTTTATGCTACGCATGGTAAC-3′	11515–11493	−	MHV C/D junction
MHV D 11511(+)	5′- **CGTCTC**AAACCACGACGTCTTTTCTATTATG-3′	11510–11534	+	MHV C/D junction
MHV D 12960(−)	5′- **CGTCTC**TTAGGATAGCATACACAATCTTACCC-3′	12966–12941	−	MHV D/E junction
MHV E 12960(+)	5′- **CGTCTC**TCCTAAGTGACTGTGATGGTCTCAAG-3′ (A T)	12961–12986	+	MHV D/E junction
MHV E 15760(−)	5′- **CGTCTC**TAGACATTAGAGTATAGGCGC-3′	15759–15739	−	MHV E/F junction
MHV F 15760(+)	5′- **CGTCTC**TGTCTATCGTGCGGACCATGTTG-3′	15754–15776	+	MHV E/F junction
MHV F 17135-mu(−)	5′- TATTCTGAAAGGTTTCAGGCACACTATAAACAC-3′ (C C)	17150–17118	−	Overlapping PCR *Esp*3I mutagenesis
MHV F 17135-mu(+)	5′- GTGCCTGAAACCTTTCAGAATAATGTGCC-3′ (G G)	17129–17157	+	Overlapping PCR *Esp*3I mutagenesis
MHV F 22740(−)	5′- **CGTCTC**TCGGACCGACTGTCACCAAATAGAAACC-3′ (A A)	22744–22717	−	MHV F/G junction
MHV G 22760(+)	5′-$(N)_6$CCCGGG**CGTCTC**GTCCGACTGTACCTATGTAG-3′ (*Esp*3I T T)		+	MHV F/G junction
MHV G 24031(−)	5′- AACGGTCTCAGTGCTAATGCTTGG-3′	24054–24031	−	MHV G end

[a] Underlined sequences represent the T7 start site, and boldface sequences represent the *Esp*3I or *Pme*I restriction sites. All primers were derived from the MHV-A59 sequence (30).

overnight in 30 mM Tris-HCl (pH 7.8)–10 mM $MgCl_2$–10 mM dithiothreitol–1 mM ATP. Appropriately sized products (A/B+C/D/E and F/G) were separated in 0.7% agarose gels as described above, isolated, and religated as described above. The final products were purified by phenol-chloroform-isoamyl alcohol (1:1:24) and chloroform extraction and precipitated under ethanol prior to in vitro transcription reactions. The full-length MHV-A59 construct is designated MHV-A59 1000. Alternatively, the seven MHV cDNA fragments were isolated, pooled, and simultaneously ligated in real time at 4°C for 18 h with T4 DNA ligase. The DNA products were phenol-chloroform extracted, precipitated, and resuspended in H_2O.

N gene transcripts may enhance coronavirus transfection efficiencies (13, 52). To provide transcripts encoding N in *trans*, the MHV-A59 N gene was amplified from the MHV G clone with primer pairs flanking the N gene ORF. The upstream primer contained an SP6 site (5′-TCGGCCTCGATGGCCATTTAG GTGACACTATAGATGTCTTTTGTTCCTGGGCAAG-3′) [a59Sp6Ng(+)] while the downstream primer introduced a 26-nucleotide oligo(T) stretch providing a poly(A) tail following in vitro transcription [5′-TCCGGA$(TTT)_8$-TTA CACATTAGAGTCATCTTCTAACC-3′] [A59Ng3′(−)]. The MHV-A59 leader RNA sequence and the 3′ noncoding sequences were not present within this construct.

RNA transfection. Full-length transcripts of the MHV-A59 1000 cDNA construct were generated in vitro as described by the manufacturer (Ambion, Austin, Tex; mMessage mMachine) with certain modifications. For 2 h at 37°C, reactions were performed with 30-μl reaction mixtures that were supplemented with 4.5 μl of a 30 mM GTP stock, resulting in a 1:1 ratio of GTP to cap analog. Similar reactions were performed with reaction mixtures with 1 μg of PCR amplicons carrying the MHV-A59 N gene sequence or Sindbis virus noncytopathic replicons encoding green fluorescent protein and a 2:1 ratio of cap analog to GTP (1). The transcripts were treated with DNase I, denatured, and separated in 0.5% agarose gels in TAE buffer containing 0.1% sodium dodecyl sulfate (SDS). Alternatively, the transcripts were either treated with 5 ng of RNase A for 15 min at room temperature, treated with DNase I, or directly electroporated into BHK or BHK-MHVR cells. Briefly, BHK and DBT cells were grown to subconfluence, trypsinized, washed twice with PBS, and resuspended in PBS at a concentration of 10^7 cells/ml. RNA transcripts were added to 800 μl of the BHK cell suspension in an electroporation cuvette, and three electrical pulses of 850 V at 25 μF were given with a Bio-Rad Gene Pulser II electroporator. The transfected BHK cells were seeded with 1.0×10^6 to 2.0×10^6 uninfected DBT cells in a 75-cm^2 flask and incubated at 37°C for 2 days. Virus progeny were then passaged in DBT cells at ~18-h intervals and twice purified by plaque assay. Alternatively, BHK-MHVR cells were electroporated with RNA transcripts as described above, and virus cytopathology and fusion were evident within ~30 h posttransfection.

Replicase gene protein expression. Replicase gene protein expression was determined as previously described (10, 19, 20, 31, 32). Briefly, monolayers of DBT cells were infected with wild-type MHV-A59 or plaque-purified molecularly cloned viruses at an MOI of 10 PFU/cell at 37°C. At 5.5 h postinfection (p.i.), 5 μg of actinomycin D/ml was added to the overlying medium. At 6 h p.i., 200 μCi of [^{35}S]Met/ml was added to the culture medium, and the cells were harvested at 8 h p.i. Cells were harvested by being washed in 10 mM Tris HCl (pH 7.4), followed by lysis in buffer containing 10 mM Tris HCl (pH 7.4), 2% SDS, 1% NP-40, and 1% sodium deoxycholate. The lysates of whole cells were adjusted to 1% SDS and immunoprecipitated with antibodies directed against the mature ORF1a proteins p28 and p65 (UP102) (20) or against MP1 (αMP1), p10 (αp10), p22 (αp22), p12 (αp12), and p15 (αp15) (10). Immunoprecipitated proteins were isolated with protein A-Sepharose beads and separated on SDS–5 to 18% gradient polyacrylamide gels. Proteins were visualized and prepared with Adobe Photoshop 5.0.

Marker mutations and sequence analysis. In contrast with the design of the TGEV infectious cDNA, the MHV-A59 construct used *Esp*3I sites that were lost during assembly of the final full-length MHV-A59 cDNA (Fig. 1). Consequently, marker mutations associated with the assembly of the full-length MHV-A59 1000 construct included changes in the three *Esp*3I sites (positions 3518, 4875, and 17138) that were removed from the wild-type virus sequence during the construction of the MHV A and F subclones and the presence of an *Rsr*II site in the HE pseudogene in the pMH54 construct (MHV G clone, position 22750) (27). Briefly, intracellular RNA was isolated from MHV-A59- or molecularly cloned virus-infected cells and used as a template for RT-PCR with primer pairs that spanned nucleotides 2020 to 5031, 16351 to 17875, or 22060 to 25416. Following RT-PCR, the amplicons were isolated from 0.8% agarose gels. Two aliquots were diluted into the appropriate restriction buffer and incubated at 37°C in the presence or absence of either *Esp*3I or *Rsr*II as described by the manufacturer (NEN). The products were separated in 0.8% agarose gels in TAE, visualized, and photographed. The remainder of the sample was cloned into Topo II TA cloning vectors as described by the manufacturer (Invitrogen), and the appropriate subclones were sequenced with an ABI automated sequencer.

RESULTS

Theoretical considerations. We have previously assembled a full-length cDNA of TGEV from which in vitro transcripts resulted in infectious virus (17, 52). Six cDNAs were isolated that spanned the entire TGEV genome, and each clone was engineered with a unique flanking interconnecting junction, which could assemble with only the adjacent cDNA subclones, resulting in an intact TGEV cDNA construct of ~28.5 kb in length. The interconnecting junctions were formed by using a subclass of restriction enzymes (e.g., *Bgl*I-**GCC**NNNN$^{\downarrow}$N**GGC**) that recognize a palindrome sequence but leave 64 (4^3) different variable ends that will assemble only with the appropriate 3-nucleotide complementary overhang generated at an identical *Bgl*I site (Fig. 1). As such, several unique *Bgl*I restriction sites were introduced into the TGEV sequence to allow for the assembly of a full-length cDNA.

We reasoned that this systematic assembly approach could be readily applied to other coronaviruses including MHV (MHV-A59), and our strategy is shown in Fig. 1. The MHV-A59 genome contains several regions of sequence toxicity-instability, which map between ~10 and 15 kb in the MHV ORF1a/ORF1b polyprotein, and a second region mapping around 5.0 kb in ORF1a (data not shown). More stable cDNAs can be isolated if the toxicity-instability domain is precisely divided into two independent subclones (52). With MHV, identification of appropriate junctions to stabilize specific cDNA clones required extensive PCR amplification and cloning and eventually confined some junctions to within a domain of a few hundred base pairs. MHV-A59 sequence constraints precluded the insertion of *Bgl*I, *Bst*XI, or a related restriction site within these narrow boundaries; therefore, a variation of this approach was used to assemble a full-length cDNA of MHV-A59.

We used a novel approach to build the unique interconnecting junctions between the MHV-A59 cDNAs that has broad and largely unappreciated molecular biology applications. The strategy is based on the unique properties associated with the restriction enzyme *Esp*3I. Like *Bst*XI, *Esp*3I is a nontraditional restriction enzyme that leaves a 4-nucleotide variable end, resulting in 256 unique potential ends. However, in contrast with these enzymes, *Esp*3I does not cleave within a palindromic sequence (5′-CGTCTCN$^{\downarrow}$NNNN-3′) but rather recognizes a strand-specific site that can be used in traditional and "No See'm" cloning strategies (Fig. 1A) (No See'm sites are named after a very small biting insect that is occasionally found on North Carolina beaches). With traditional approaches, *Esp*3I sites can be oriented to re-form the recognition site in recombinant viruses following in vitro ligation of two adjacent MHV cDNAs. However, a simple reverse orientation places both *Esp*3I sites at the ends of the viral cDNAs, with the variable overhang generated from the virus sequence. Upon cleavage and ligation with the adjoining fragment, both *Esp*3I sites are lost from the final product, leaving the exact MHV-A59 sequence at the junction. Restriction enzymes encoding similar properties include *Sap*I, *Bsa*I, and *Bsm*I and others (39).

Assembly of a full-length infectious cDNA of MHV-A59. We reasoned that these enzymatic properties would allow for the assembly of a full-length MHV-A59 cDNA with minimal sequence alteration at the junctions between component clones. As the wild-type MHV-A59 genome contained three *Esp*3I sites, silent mutations were inserted to disrupt these sites around nucleotide positions 3518 and 4875 in MHV A and position 17138 in the MHV F cDNA fragment. Breaking the sequence at nucleotides 4882, 11510, 12961, and 15754 reduced the toxicity-instability domains in the MHV-A59 cDNAs. Consequently, seven MHV-A59 cDNAs that contained unique *Esp*3I or *Bgl*I interconnecting junctions were isolated by using specific primer pairs and RT-PCR (Fig. 1B). The introduced *Esp*3I sites did not alter the amino acid sequence because they were eliminated during the assembly of the full-length genomic cDNA (Table 1). The MHV-A59 A cassette (~4.9 kb) contained a T7 RNA polymerase start at the 5′ end and terminated in an *Esp*3I site located at position 4882. The resulting 4-nucleotide CAAA overhang formed the MHV A/B junction. The MHV-A59 B fragment (~4.6 kb) contained the same *Esp*3I site at its 5′ end and terminated in a natural *Bgl*I site located at position 9555 in the MHV-A59 genome. The resulting 3-nucleotide TAA overhang formed the basis of the unique B/C junction. The MHV-A59 C fragment (~2.0 kb) encoded the *Bgl*I site at the 5′ end and terminated in an *Esp*3I site at position 11510. The resulting AACC sequence formed the basis for the MHV C/D junction. The MHV-A59 D fragment (~1.5 kb) encoded the position 11510 *Esp*3I site and terminated in an *Esp*3I site that was engineered at position 12961. To prevent spurious assembly with other fragments, we engineered in a CCTA sequence (wild-type sequence is ACTT) that formed the basis for the MHV D/E interconnecting junction. This did not change the protein sequence of MHV-A59. The MHV-A59 E fragment (~2.8 kb) terminated in an *Esp*3I site at position 15754 with the resulting GTCT sequence serving as the E/F junction (Fig. 1C). The MHV F cDNA clone (~7.0 kb) terminated in an *Esp*3I site located in the HE glycoprotein gene at position 22739 and left a TCCG junction (27, 30). This included the introduction of a T-to-C alteration at position 22742. The MHV-A59 G fragment (~8.7 kb) was derived from the pMH54 construct used in targeted recombination (kindly provided by Paul Masters). For our purposes, pMH54 was modified by introducing an *Esp*3I site at nucleotide 22740 partially overlapping with an *Rsr*II site that is present in the pMH54 construct (Table 1). The MHV F and G cDNAs can be assembled with either the *Esp*3I or *Rsr*II sites. Primer pairs used to introduce these restriction sites and form the unique interconnecting junctions are shown in Table 2.

Using RT-PCR and the primer pairs shown in Table 2, we successfully isolated stable clones that spanned the MHV genome. Importantly, the clones encoding the toxic domains (MHV B, C, and D) were most stable at 30°C in pSMART vectors. Three to seven independent clones of each were sequenced, and a consensus cDNA clone was established for each of the MHV A, B, C, D, E, and G cDNAs by standard recombinant DNA techniques. The final consensus sequence in our construct contained two amino acid changes from the published sequence, a T-to-C change at position 5304 (Ser-Pro) and an A-to-T change at position 6796 (Lys-Met) (30).

To assemble a full-length cDNA of the MHV genome, plasmids were digested and the appropriate-sized inserts were isolated from agarose gels (Fig. 2A). Two assembly strategies were devised. In the first approach, the MHV A and B; C, D, and E; and F and G fragments were ligated overnight in the

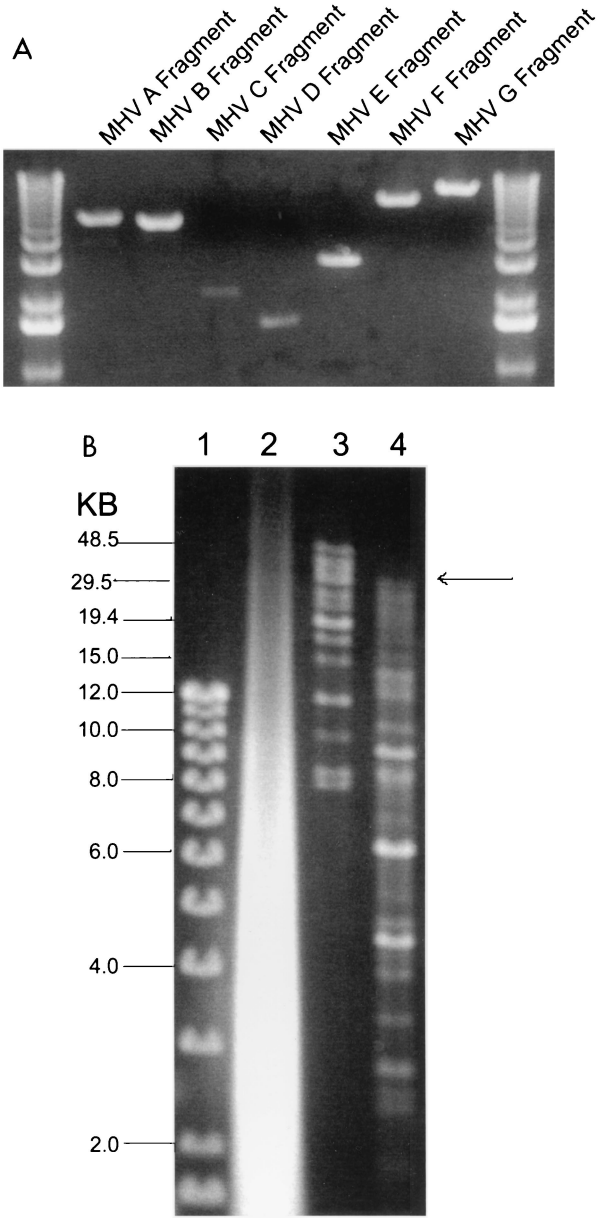

FIG. 2. Assembly of an MHV-A59 full-length cDNA. (A) Plasmid DNAs were restricted with the appropriate enzymes and separated in 0.8% agarose gels, and the MHV cDNAs were purified from gels. The sizes (in kilobases) of the MHV fragments are as follows: A, ~4.8; B, ~4.3; C, ~2.0; D, ~1.5; E, ~2.8; F, ~7.0; and G, ~8.7. DNA molecular size markers flank the MHV cDNAs. (B) The purified cDNAs were pooled and incubated with T4 DNA ligase for 12 h at 4°C. One-thirtieth of the assembled products were separated in 0.5% agarose gels overnight at 15 V. Lane 1, small-molecular-size 1-kb markers; lane 2, in vitro transcripts derived from MHV-A59 1000 and treated with DNase I; lane 3, high-molecular-weight markers; lane 4, shotgun-assembled MHV-A59 component cDNAs. The arrow indicates the presence of large-molecular-size ~31.5-kb cDNA.

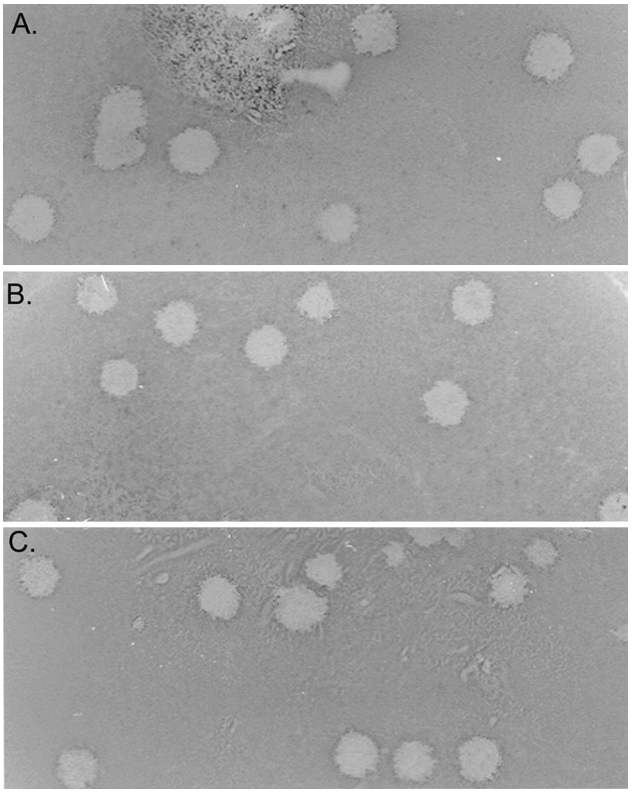

FIG. 3. Molecularly cloned virus plaque morphology. Cultures of BHK cells were electroporated with MHV-A59 1000 full-length transcripts or MHV-A59 1000 cDNA and seeded with DBT cells in 75-cm^2 flasks. Virus progeny were purified by plaque assay, and virus stocks were grown as described in Materials and Methods. The figure shows the plaque morphologies of wild-type MHV-A59 virus (A) and molecularly cloned icMHV-A59#1 (B) and icMHV-A59#2 (C) virus.

presence of T7 DNA ligase. The ligation products were isolated from agarose gels, and the MHV A/B, C/D/E, and F/G fragments were pooled and ligated overnight. The final products were purified by phenol-chloroform-isoamyl alcohol extraction and precipitated under ethanol, and an aliquot was separated in agarose gels (data not shown). In the second approach, purified MHV A, B, C, D, E, F, and G fragments were pooled and ligated overnight at 4°C. The products were phenol-chloroform extracted and concentrated by precipitation (Fig. 2B). In both approaches, an appropriately sized full-length MHV-A59 cDNA of approximately 31.5 kb in length (MHV-A59 1000) was generated as well as some assembly intermediates, especially evident during simultaneous ligation. Capped T7 transcripts were synthesized, treated with DNase, and analyzed in 0.5% agarose gels (Fig. 2B). Low levels of high-molecular-weight transcript were evident following T7 transcription of ligated fragments in vitro. DNase treatment removed the MHV-A59 full-length cDNA as well as the incomplete assembly intermediates (data not shown).

Transfection and recovery of infectious virus. BHK cells are nonpermissive for MHV-A59 infection because of a block in virus docking and entry. However, BHK cells were used because of high transfection efficiencies with infectious coronavirus genomic RNAs (48, 52). As previous studies with TGEV and IBV have demonstrated that N transcripts may enhance transfection efficiencies of genome-length transcripts (13, 52), we included MHV N transcripts in our initial transfection studies. As BHK cells will function as single-hit hosts, the transfected BHK cells were seeded into 75-cm^2 flasks containing 1.0×10^6 to 2.0×10^6 DBT cells, which are permissive for MHV replication. By 36 h, cytopathology was evident in the transfected cultures. When the media from these cultures were passaged into a fresh flask of DBT cells, viral cytopathology was evident by 12 h p.i., and molecularly cloned virus produced plaques in DBT cells and reached high titers of 10^7 PFU/ml. No infectious virus or cytopathology was evident from MHV-A59 1000 DNA-transfected cultures or from RNase A-treated transcripts (data not shown). Several plaques were isolated from these passage 1 cultures. Titers of molecularly cloned virus stocks were determined at 0.9×10^8 to 2.0×10^8 PFU/ml (icMHV-A59#1, icMHV-A59#2, icMHV-A59#3, icMHV-A59#4, and icMHV-A59#5) and had similar plaque morphology as did wild-type virus (Fig. 3).

BHK-MHVR cells express the receptor for MHV-A59 docking and entry into cells and are susceptible to infection (15, 16). Consequently, transfection of MHV-A59 1000 transcripts into BHK-MHVR cells allows for additional rounds of progeny virion multiplication. To determine if MHV-A59 N transcripts enhanced the infectivity of full-length transcripts, cultures of BHK-MHVR cells were transfected in the presence or absence of N transcripts, and the cultures were fixed at 16 and 25 h p.i. By fluorescent antibody staining, cotransfected cultures displayed significantly increased amounts of viral antigen at 16 and 25 h p.i. compared with cultures transfected with MHV-A59 1000 transcripts alone (Fig. 4). Viral antigen expression was noted within regions of viral cytopathology and fusion indicative of S glycoprotein expression. Consonant with these findings, virus titers at 25 h p.i. were 1.9×10^4 and 2.8×10^5 PFU/ml in the absence or presence of N transcripts, respectively. These data indicate that N transcripts are not necessary for infectivity of MHV-A59 1000 transcripts, although infectivity is enhanced 10- to 15-fold.

Phenotype of molecularly cloned viruses. Cultures of DBT cells were infected with wild-type MHV-A59 and several molecularly cloned viruses at an MOI of 10 for 1 h at room temperature, and virus samples were harvested at the indicated times. Wild-type and molecularly cloned viruses had indistinguishable growth characteristics in DBT cells and reached titers of $\sim 2.0 \times 10^8$ PFU/ml within 16 h p.i. (Fig. 5). Wild-type MHV-A59 infection in DBT cells is sensitive to blockade with monoclonal antibody CC1, which binds the N-terminal domain of MHVR (23). As shown in Fig. 5A, both wild-type MHV-A59 and molecularly cloned viruses were sensitive to CC1 blockade, consistent with the notion that MHVR was being recognized as a receptor for docking and entry into DBT cells. To further test this hypothesis, BHK-MHVR cells were pretreated with CC1 monoclonal antibodies and then infected with wild-type MHV-A59 or various molecularly cloned viruses (Fig. 5B). MHV-A59 and the molecularly cloned viruses could not replicate in BHK cells unless the MHVR receptor was expressed and present on the surface of cells (Fig. 5C). Moreover, pretreatment of BHK-MHVR cells with CC1 blocked the replication of both wild-type MHV-A59 and the molecularly cloned viruses (Fig. 5B). These data indicate that the molecularly cloned viruses used MHVR as a receptor for docking and entry.

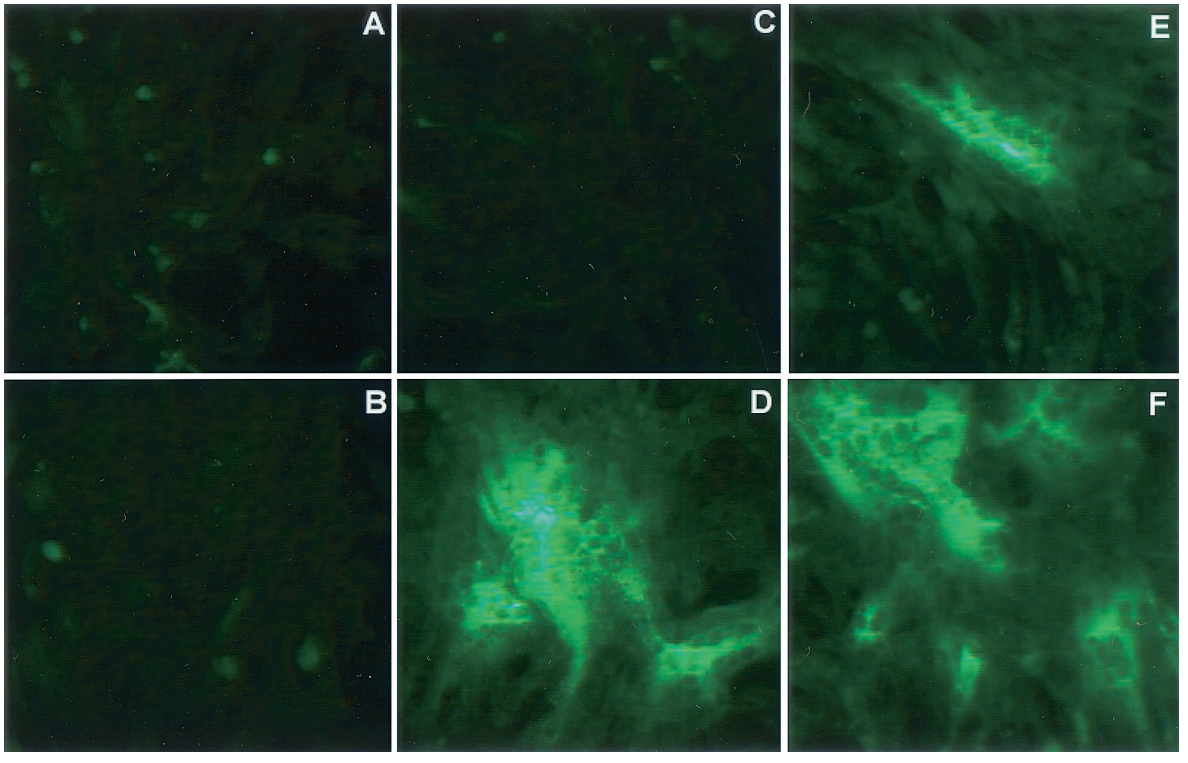

FIG. 4. Viral antigen expression in the presence or absence of nucleocapsid transcripts. Cultures of BHK-MHVR cells were electroporated with MHV-A59 1000 alone or with a mixture of MHV-A59 1000 and N gene transcripts as described in Materials and Methods. In LabTek chambers, 2×10^5 cells were seeded and fixed at 16 and 25 h posttransfection. With murine antiserum against MHV-A59, fluorescent antibody staining demonstrated that MHV-A59 1000 transcripts were infectious in the presence or absence of N transcripts. (A B) Untransfected culture at 16 h; (B) untransfected culture at 25 h; (C) culture transfected in the absence of N transcripts, at 16 h; (C) culture transfected in the presence of N transcripts, at 16 h; (E) culture transfected in the absence of N transcripts, at 25 h (F) culture transfected in the presence of N transcripts, at 25 h.

MHV replicase protein expression. Reverse genetic approaches are needed to determine the function of the gene 1 replicase proteins in coronavirus replication and pathogenesis. Consequently, we compared the processing, mobility, and expression of the ORF1a replicase proteins in cultures of DBT cells that had been infected with wild-type MHV-A59 or ic-MHV-A59 at an MOI of 10. The cultures were radiolabeled with [^{35}S]methionine from 6 to 8 h p.i. Whole-cell lysates of infected cells were immunoprecipitated with antisera directed against previously characterized MHV-A59 ORF1a replicase proteins (Fig. 6). The amino-terminal ORF1a proteins p28 and p65 were detected in similar amounts and mobilities in ic-MHV-A59 and wild-type virus. Further analysis of icMHV-A59 demonstrated that the mature ORF1a replicase proteins MP1, p12, p22, p10, and p15 were identical in amount and mobility to those in wild-type-virus-infected cells. These data also indicated that the proteinases responsible for these protein cleavages, PLP1, PLP2, and 3CLpro, functioned normally in the molecularly cloned viruses. Thus, viruses recovered from the genome-length cDNA were capable of normal replicase protein processing and expression.

Identification of marker mutations in molecularly cloned viruses. Molecularly cloned viruses should contain wild-type sequence at most of the junctions but will have lost the three *Esp*3I sites that were removed from the MHV-A59 A and G fragments (positions 3518, 4875, and 17138). In addition, molecularly cloned viruses should carry an *Rsr*II site in the HE glycoprotein pseudogene that was present in the original pMH54 construct (position 22750). Consequently, wild-type MHV-A59 and various molecularly cloned viruses were inoculated into DBT cells, and intracellular RNA was isolated at 6 h p.i. With RT-PCR, several amplicons were generated that spanned either the A/B and G/F junctions or the marker mutations used to eliminate the naturally occurring *Esp*3I sites in the MHV genome (Fig. 7). Results of restriction fragment length polymorphism analysis demonstrated that the three expected *Esp*3I sites, but not the *Rsr*II site, were present in the wild-type MHV-A59 genome (Fig. 7). In contrast, molecularly cloned MHV-A59 virus contained the unique marker mutations that had eliminated these three *Esp*3I restriction sites in the MHV-A59 1000 full-length cDNA (Fig. 7). Importantly, molecularly cloned viruses contained the expected *Rsr*II site that was present in the MHV G fragment and contained wild-type sequence at each of the *Esp*3I junctions used to assemble the full-length cDNA (Fig. 7 and 8). The appropriate PCR products were subcloned and sequenced, demonstrating that the appropriate mutations were present in the viruses isolated from the infectious construct (Fig. 8). Clearly, MHV-A59 1000 transcripts were infectious and produced virus which contained not only the appropriate marker mutations but also wild-type virus sequence at each of the junctions.

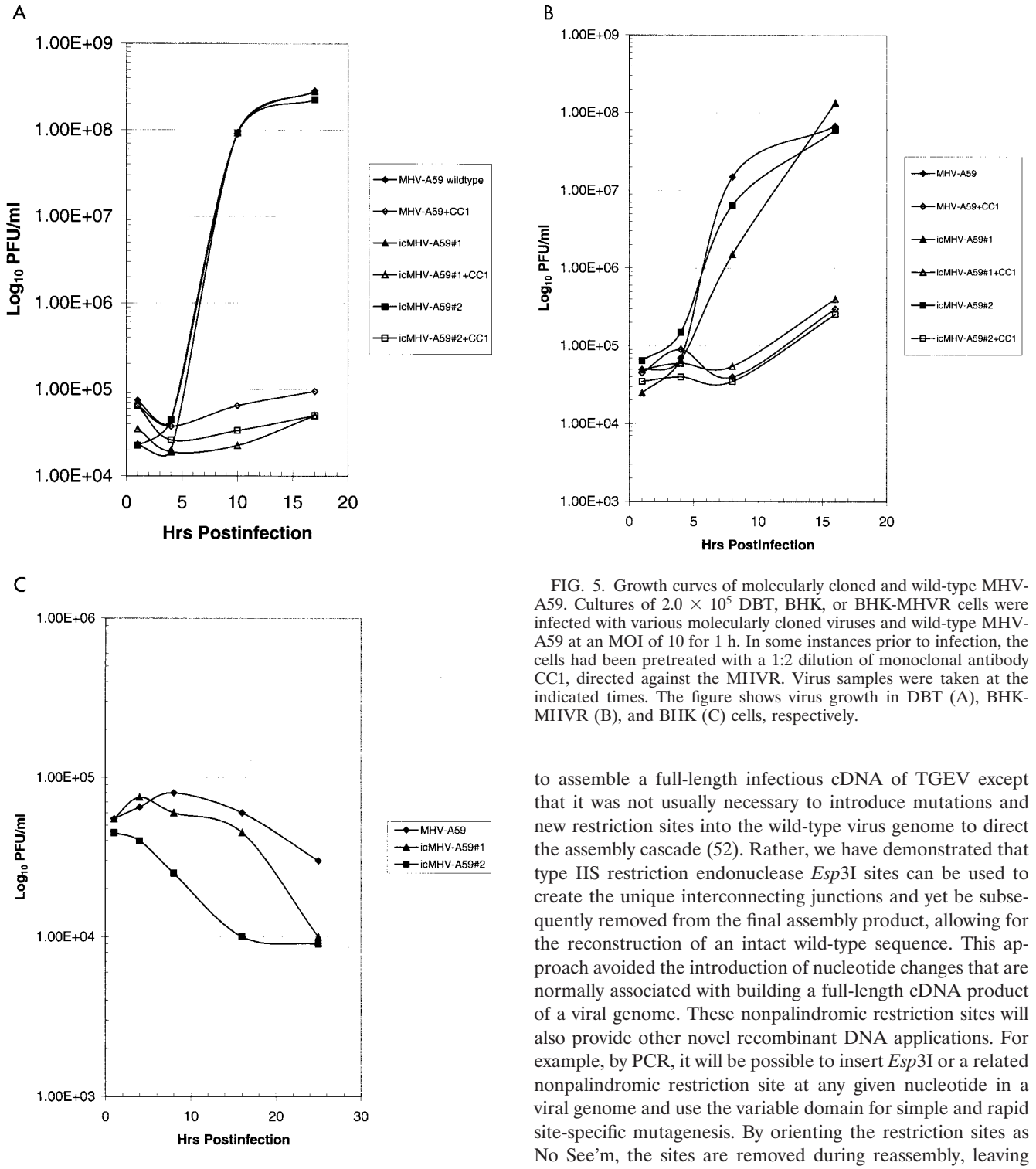

FIG. 5. Growth curves of molecularly cloned and wild-type MHV-A59. Cultures of 2.0×10^5 DBT, BHK, or BHK-MHVR cells were infected with various molecularly cloned viruses and wild-type MHV-A59 at an MOI of 10 for 1 h. In some instances prior to infection, the cells had been pretreated with a 1:2 dilution of monoclonal antibody CC1, directed against the MHVR. Virus samples were taken at the indicated times. The figure shows virus growth in DBT (A), BHK-MHVR (B), and BHK (C) cells, respectively.

DISCUSSION

In this study we report the first reverse genetic system for a group II coronavirus, MHV-A59, which allows for the successful recovery of infectious virus following assembly of a genome-length cDNA from a series of contiguous cDNA subclones. The approach was similar to the strategy that was used to assemble a full-length infectious cDNA of TGEV except that it was not usually necessary to introduce mutations and new restriction sites into the wild-type virus genome to direct the assembly cascade (52). Rather, we have demonstrated that type IIS restriction endonuclease *Esp*3I sites can be used to create the unique interconnecting junctions and yet be subsequently removed from the final assembly product, allowing for the reconstruction of an intact wild-type sequence. This approach avoided the introduction of nucleotide changes that are normally associated with building a full-length cDNA product of a viral genome. These nonpalindromic restriction sites will also provide other novel recombinant DNA applications. For example, by PCR, it will be possible to insert *Esp*3I or a related nonpalindromic restriction site at any given nucleotide in a viral genome and use the variable domain for simple and rapid site-specific mutagenesis. By orienting the restriction sites as No See'm, the sites are removed during reassembly, leaving only the desired mutation in the final DNA product. The dual properties of strand specificity and a variable end overhang that can be tailored to match any sequence allow for *Esp*3I sites to be engineered as universal connectors that can be joined with any other 4-nucleotide restriction site overhang (e.g., *Eco*RI, *Pst*XI, and *Bam*HI). Alternatively, No See'm sites can be used to insert foreign genes into viral, eukaryotic, or microbial genomes or vectors, simultaneously removing all ev-

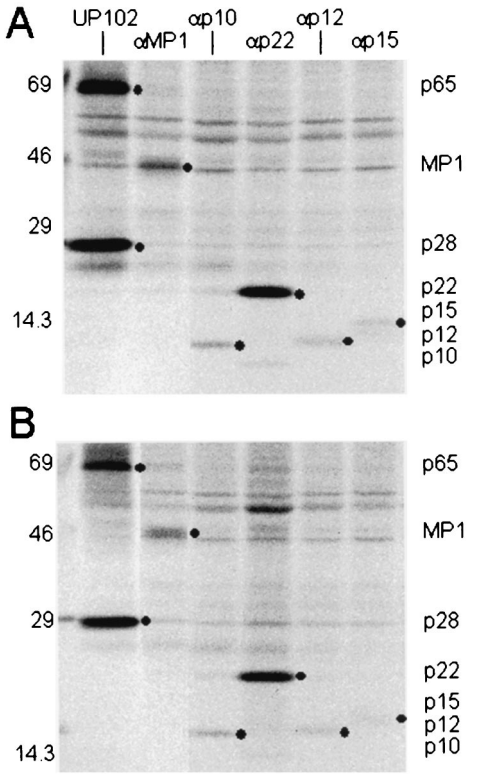

FIG. 6. Expression of replicase proteins of wild-type MHV-A59 and icMHV-A59. Wild-type MHV-A59 and icMHV-A59#1 were inoculated onto monolayers of DBT cells at an MOI of 10 for 1 h. Cells were maintained for 5.5 h in Dulbecco modified Eagle medium–2% fetal calf serum, and at 5.5 h, the media were replaced with Dulbecco modified Eagle medium that lacked methionine and cysteine and contained 2% fetal calf serum. Actinomycin D (2 μg/ml) was also added at 5.5 h p.i., and at 6.0 h, the cultures were pulsed with [^{35}S]Met for 2 h. Cells were lysed at 8 h p.i. in lysis buffer containing 10 mM Tris-HCl, 1% NP-40, and 2% SDS. Immunoprecipitation of replicase proteins was performed in 200-μl reaction mixtures containing lysate from ~10^5 cells in 10 mM Tris–1% NP-40–1% SDS. The specificities and sensitivities of the antibodies directed against p28/p65 (UP102), MP1 (αMP1), 3CLpro (B3), p12 (αp1a-12), p22 (αp22), p10 (αp1a-10), and p15 (αp1a-15) have been reported previously (10, 19, 20, 31, 32). Molecular weight markers are shown to the left of each gel, and black circles identify the various MHV replicase protein products.

idence of the restriction sites that were used in the recombinant DNA manipulation.

The MHV-A59 systematic assembly strategy involves seven contiguous cDNAs and offers several unique advantages as a reverse genetic system for coronaviruses. These include (i) reduced sequence complexity and the corresponding increased availability of rare restriction sites that allow for rapid reverse genetic manipulations in individual cassettes compared with a full-length genome clone; (ii) sequence compartmentalization in individual cassettes, minimizing the possibility of spurious second-site mutations and recombination that may occur frequently in large inserts during recombinant DNA manipulations; (iii) the disruption of the MHV toxic regions, which are normally unstable in microbial vectors; (iv) avoidance of the introduction of mutations that create new restriction sites in the viral sequence; (v) compatibility with vaccinia virus or bacterial artificial chromosome vectors; and (vi) the fact that the theoretical limits of the assembly cascade with the rarest cutters like *Sap*I greatly exceed the sizes of most million-base-pair microbial genomes as well as all RNA and DNA viral genomes described to date. As such, many DNA and RNA virus and microbial genomes could also be reassembled from component clones by this approach.

We purposely introduced several silent changes to remove preexisting *Esp*3I sites that resided within the MHV-A59 genome sequence and to distinguish between molecularly cloned and wild-type viruses. In one instance, the *Esp*3I site at position 4875 was removed because it left a TTAA overhang that would have prevented the directionality of assembly. The other *Esp*3I sites were removed to minimize the total number of MHV-A59 subclones used in the assembly cascade. In two instances, we inserted silent mutations into the *Esp*3I overhang to maximize sequence specificity and directionality at a particular junction (Tables 1 and 2), but this could be circumvented by choosing slightly different junction sites. The MHV cDNA cassettes can be ligated systematically as described for TGEV or simultaneously. Although numerous incomplete assembly intermediates were evident, our demonstration that simultaneous ligation of seven cDNAs will result in full-length cDNA will

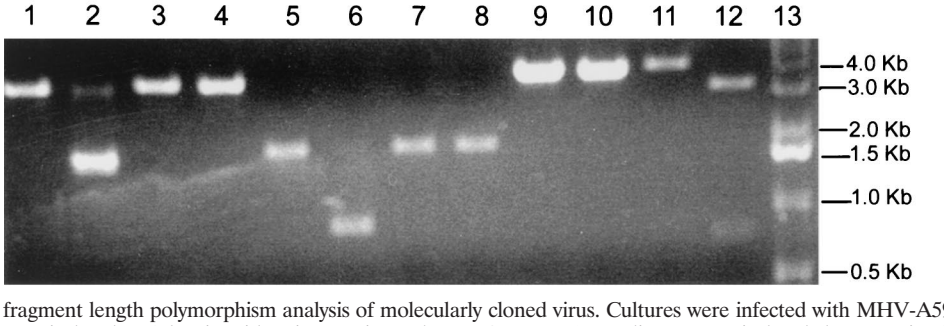

FIG. 7. Restriction fragment length polymorphism analysis of molecularly cloned virus. Cultures were infected with MHV-A59 or icMHV-A59#1, and intracellular RNA was isolated at 8 h p.i. With primer pairs and RT-PCR, cDNA amplicons were isolated that contained the various marker mutations that had been inserted into the component clones. The purified wild-type MHV-A59 and icMHV-A59#1 amplicons were restricted with *Esp*3I or *Rsr*II and separated in 0.8% agarose gels. Lane 1, wild-type A59 amplicon from nucleotides 2020 to 5031, uncut; lane 2, wild-type A59 amplicon from nucleotides 2020 to 5031 digested with *Esp*3I; lane 3, icMHV-A59#1 amplicon from nucleotides 2020 to 5031, uncut; lane 4, icMHV-A59#1 amplicon from nucleotides 2020 to 5031, *Esp*3I digested; lane 5, wild-type A59 amplicon from nucleotides 16351 to 17875, uncut; lane 6, wild-type A59 amplicon from nucleotides 16351 to 17875 restricted with *Esp*3I; lane 7, icMHV-A59#1 amplicon from nucleotides 16351 to 17875, uncut; lane 8, icMHV-A59#1 amplicon from nucleotides 16351 to 17875 restricted with *Esp*3I; lane 9, wild-type A59 amplicon from nucleotides 22060 to 25416, uncut; lane 10, wild-type A59 amplicon from nucleotides 22060 to 25416 restricted with *Rsr*II; lane 11, icMHV-A59#1 amplicon from nucleotides 22060 to 25416, uncut; lane 12, icMHV-A59#1 amplicon from nucleotides 22060 to 25416 restricted with *Rsr*II; lane 13, 1-kb ladder.

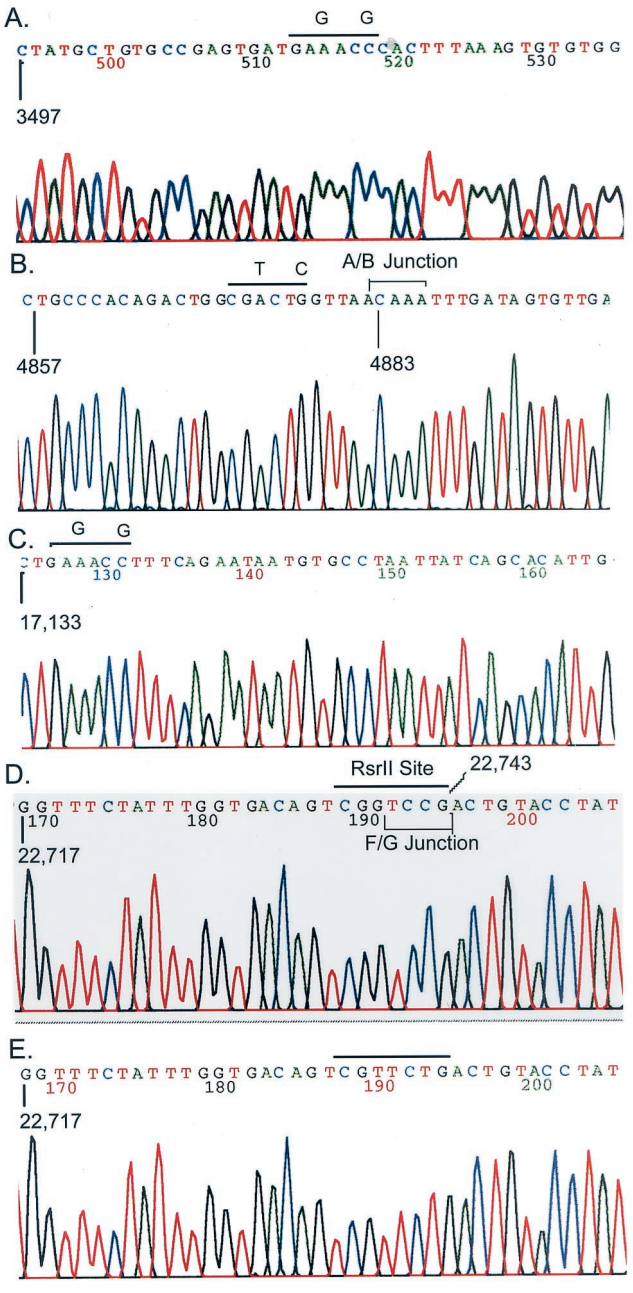

FIG. 8. Identification of marker mutations in recombinant virus. Various icMHV-A59#1 or wild-type virus amplicons were subcloned into Topo II vectors and sequenced. (A) icMHV-A59#1 sequence across the mutated 3512 *Esp*3I site; (B) icMHV-A59#1 sequence across the mutated 48 *Esp*3I site and the MHV A/B junction; (C) icMHV-A59#1 sequence across the mutated 17 *Esp*3I site; (D) icMHV-A59#1 sequence across the *Rsr*II site and MHV F/G junction; (E) wild-type MHV-A59 sequence across the same domain as shown in panel D. Overlined sequences include the mutated restriction sites and the corresponding wild-type nucleotides at these positions. In panels B and D, the bracketed sequences represent the MHV A/B and F/G junction domains, respectively. Note that all evidence of the *Esp*3I site, which had been engineered into the sequence, is gone.

simplify the complexity of the assembly strategy. At this time, there is no evidence to indicate that this approach might introduce spurious mutations or genome rearrangements from aberrant assembly cascades. However, it is possible that such variants might arise following RNA transfection, as a consequence of high-frequency MHV RNA recombination between incomplete and genome-length transcripts (35). It is likely that such variants would be replication impaired and rapidly outcompeted by wild-type virus. A second limitation is that the yield of full-length cDNA product is reduced, resulting in less robust transfection efficiencies than those of the more traditional systematic assembly method.

The group I and III coronaviruses appear to encode a single toxicity-instability region in ORF1a (3, 52). In contrast, MHV-A59 contains several regions in ORF1, particularly between nucleotides 9555 and 15754, that are highly unstable and/or toxic in many high- or low-copy-number plasmids in *Escherichia coli*. To solve this problem, we took advantage of the observation that toxicity can be significantly reduced if the domains are bisected into two distinct subclones and if the microbial vectors are propagated at 30°C. In MHV-A59, the toxic regions map within the small 3CLpro cleavage products at the C terminus of ORF1a, near the PLP about 5.0 kb in ORF1a, and at the N terminus of ORF1b (10, 19, 20, 25, 31, 32). Instability appears to be associated with expression, as this entire domain (nucleotides 9555 to 15754) is stable in yeast vectors (pYES2.1 Topo TA cloning kit from Invitrogen) that maintain tight regulation over foreign gene expression (B. Yount et al., unpublished data). Importantly, the MHV B, C, and D clones were most stable in low-copy-number pSMART plasmids, which are transcription- and translation-free cloning vectors. These vectors lack a β-galactosidase promoter, and the MHV inserts are flanked by strong transcriptional stops, providing further support for the hypothesis that toxicity is expression linked. We are determining if the entire C-to-E domain can be stably cloned into pSMART vectors. As an alternative, preliminary data also suggest that the MHV B, C, and D inserts may be more stable in Topo II/pGEM vectors in the presence of glucose, presumably from the induction of catabolite repression.

Coronaviruses have been demonstrated elsewhere to package low concentrations of subgenomic mRNAs, especially N transcripts, and several studies have suggested that N transcripts may function in transcription and replication and are tightly associated with the replication complex (7, 19, 42, 47). Previous studies in our laboratory with TGEV, and then in other laboratories with IBV, have shown that N transcripts enhance the infectivity of transcripts derived from coronavirus full-length cDNAs (13, 52). With IBV, but not TGEV or HCV 229E, N transcripts are absolutely essential for full-length transcript infectivity (13). In this study, N transcripts enhanced the infectivity of full-length MHV-A59 transcripts by 10- to 15-fold as evidenced by increased viral antigen expression and virus titers at 25 h p.i. It is unclear whether MHV N transcripts, N protein, or both are essential for increased virus yields following electroporation or whether this effect would be observed with transcripts of unrelated genes. Previous reports indicate that N transcripts do not appear absolutely necessary for HCV 229E subgenomic RNA transcription (49). Additional studies are needed to determine exactly how N transcripts enhance infectivity of coronavirus genome-length transcripts in vitro.

MHV-A59 has long served as a model system for studying coronavirus genetics, polymerase function, replication, transcription, receptor usage, assembly and release, and pathogen-

esis (29). The availability of a full-length infectious cDNA of MHV-A59 will allow for reverse genetic applications throughout the entire MHV genome. Virus recovered from the infectious construct replicated as efficiently as did wild-type virus, approached titers of 10^8 PFU/ml within 16 h p.i., and, importantly, contained the marker mutations engineered into several of the component clones. Molecularly cloned virus utilized MHVR as a receptor for docking and entry into cells, was sensitive to blockade with monoclonal antibodies against MHVR, and displayed similar host range restriction as did the wild-type virus. Consequently, the reverse genetic system will prove applicable to studying MHV-A59 receptor interactions as well as elucidating the mechanisms of coronavirus host range expansion and persistence (5, 6, 15, 21, 22, 23, 41).

Further, the use of a cassette approach to construct infectious cDNAs of MHV-A59 will allow for the precise and rapid introduction of mutations into regions of the genome that are currently inaccessible by targeted RNA recombination approaches, specifically the entire 5′ two-thirds of the genome and notably the MHV replicase gene, gene 1. Although a great deal has been learned concerning the expression, processing, targeting, and interactions of replicase gene proteins, it has not been possible to determine the functions of most of them. Novel functions that must be encoded include proteins that regulate MHV discontinuous transcription, high-frequency RNA recombination, and positive- and negative-strand RNA synthesis. As arteriviruses use a similar transcriptional strategy and yet encode a replicase gene that is one-third to one-half the size of the MHV gene, it seems likely that novel nidovirus gene 1 functions will be encoded in the coronavirus replicase gene that assist in the replication of large RNA genomes. The approaches described here will allow direct reverse genetic studies of individual replicase gene proteins, as well as any combination of proteins because of the ability to mix and match different mutated gene fragments.

In summary, we have established a reverse genetic system for the group II coronavirus MHV-A59. The strategy used in the assembly of this infectious cDNA could be applied to other important group II coronaviruses like bovine coronavirus, an important pathogen of cattle, and HCV OC43, which is an important cause of upper respiratory tract infections in humans. Moreover, it will be possible to target MHV to multiple species by simple replacement of the S glycoprotein gene (27), allowing for the development of MHV-A59 as a vaccine vector in domesticated animals and humans. Host range variants of MHV may recognize human CEA genes for docking and entry, allowing for virus targeting of unique cell populations in humans (5, 6, 36). These features, coupled with a transcriptional strategy that will likely allow for regulated expression of multiple genes from the genome, should allow for the use of coronaviruses as heterologous vaccine vectors in humans and animals (17, 24).

ACKNOWLEDGMENTS

We thank Xiaotao Lu for outstanding technical support and Kris Curtis, Patrick Harrington, Sonnie Lambeth, and William McRoy for critical review of the manuscript. We thank Paul Masters for kindly providing the pMH54 plasmid that carried a functional 3′ end of the MHV-A59 genome.

This research was supported by research grants from the National Institutes of Health, AI23946 and GM63228 to R.S.B., AI26603 to M.R.D., and AI17418 to S.R.W.

REFERENCES

1. **Agapov, E. V., I. Frolov, B. D. Lindenbach, B. M. Pragai, S. Schlesinger, and C. M. Rice.** 1998. Noncytopathic sindbis virus RNA vectors for heterologous gene expression. Proc. Natl. Acad. Sci. USA **95:**12989–12994.
2. **Ahlquist, P., R. French, M. Janda, and L. S. Loesch-Fries.** 1984. Multicomponent RNA plant virus infection derived from cloned viral cDNA. Proc. Natl. Acad. Sci. USA **81:**7066–7070.
3. **Almazan, F., J. M. Gonzalez, Z. Penzes, A. Izeta, E. Calvo, J. Plana-Duran, and L. Enjuanes.** 2000. Engineering the largest RNA virus genome as an infectious bacterial artificial chromosome. Proc. Natl. Acad. Sci. USA **97:**5516–5521.
4. **Baric, R. S., and B. Yount.** 2000. Subgenomic negative-strand function during mouse hepatitis virus infection. J. Virol. **74:**4039–4046.
5. **Baric, R. S., E. Sullivan, L. Hensley, B. Yount, and W. Chen.** 1999. Persistent infection promotes cross-species transmissibility of mouse hepatitis virus. J. Virol. **73:**638–649.
6. **Baric, R. S., B. Yount, L. Hensley, S. A. Peel, and W. Chen.** 1997. Episodic evolution mediates interspecies transfer of a murine coronavirus. J. Virol. **71:**1946–1955.
7. **Baric, R. S., G. W. Nelson, J. O. Fleming, M. M. C. Lai, and S. A. Stohlman.** 1988. Interactions between coronavirus nucleocapsid protein and viral RNAs: implications for viral transcription. J. Virol. **62:**4280–4287.
8. **Bonilla, P. J., A. E. Gorbalenya, and S. R. Weiss.** 1994. Mouse hepatitis virus strain A59 RNA polymerase gene ORF1a: heterogeneity among MHV strains. Virology **198:**736–740.
9. **Bonilla, P. J., S. A. Hughes, and S. R. Weiss.** 1997. Characterization of a second cleavage site and demonstration of activity in *trans* by the papain-like proteinase of the murine coronavirus mouse hepatitis virus strain A59. J. Virol. **71:**900–909.
10. **Bost, A. G., R. H. Carnahan, X. T. Lu, and M. R. Denison.** 2000. Four proteins processed from the replicase gene polyprotein of mouse hepatitis virus colocalize in the cell periphery and adjacent to sites of virion assembly. J. Virol. **74:**3379–3387.
11. **Boyer, J. C., and A. L. Haenni.** 1994. Infectious transcripts and cDNA clones of RNA viruses. Virology **198:**415–426.
12. **Bredenbeek, P. J., C. J. Pachuk, A. F. Noten, J. Charite, W. Luytjes, S. R. Weiss, and W. J. Spaan.** 1990. The primary structure and expression of the second open reading frame of the polymerase gene of the coronavirus MHV-A59; a highly conserved polymerase is expressed by an efficient ribosomal frameshifting mechanism. Nucleic Acids Res. **18:**1825–1832.
13. **Casais, R., V. Thiel, S. G. Siddell, D. Cavanagh, and P. Britton.** 2001. Reverse genetic system for the avian coronavirus infectious bronchitis virus. J. Virol. **75:**12359–12369.
14. **Cavanagh, D., and M. C. Horzinek.** 1993. Genus Torovirus assigned to the coronaviridae. Arch. Virol. **128:**395–396.
15. **Chen, W., and R. S. Baric.** 1996. Molecular anatomy of mouse hepatitis virus persistence: coevolution of increased host resistance and virus virulence. J. Virol. **70:**3947–3960.
16. **Chen, W., V. J. Madden, R. Bagnell, Jr., and R. S. Baric.** 1997. Host-derived intracellular immunization against mouse hepatitis virus infection. Virology **228:**318–332.
17. **Curtis, K. M., B. Yount, and R. S. Baric.** 2001. Heterologous gene expression from transmissible gastroenteritis virus replicon particles. J. Virol. **76:**1422–1434.
18. **de Haan, C. A. M., H. Vennema, and P. J. M. Rottier.** 2000. Assembly of the coronavirus envelope: homotypic interactions between the M proteins. J. Virol. **74:**4967–4978.
19. **Denison, M. R., W. J. Spaan, Y. van der Meer, C. A. Gibson, A. C. Sims, B. Prentice, and X. T. Lu.** 1999. The putative helicase of the coronavirus mouse hepatitis virus is processed from the replicase gene polyprotein and localizes in complexes that are active in viral RNA synthesis. J. Virol. **73:**6862–6871.
20. **Denison, M. R., S. A. Hughes, and S. R. Weiss.** 1995. Identification and characterization of a 65 kDa protein processed from the gene 1 polyprotein of the murine coronavirus MHV-A59. Virology **207:**316–320.
21. **Dveksler, G. S., C. W. Dieffenbach, C. B. Cardellichio, K. McCuaig, M. N. Pensiero, G.-S. Jiang, N. Beauchemin, and K. V. Holmes.** 1993. Several members of the mouse carcinoembryonic antigen-related glycoprotein family are functional receptors for the coronavirus mouse hepatitis virus-A59. J. Virol. **67:**1–8.
22. **Dveksler, G. S., M. N. Pensiero, C. B. Cardellichio, R. K. Williams, G.-S. Jiang, K. V. Holmes, and C. W. Dieffenbach.** 1991. Cloning of the mouse hepatitis virus (MHV) receptor: expression in human and hamster cell lines confers susceptibility to MHV. J. Virol. **65:**6881–6891.
23. **Dveksler, G. S., M. N. Pensiero, C. W. Dieffenbach, C. B. Cardellichio, A. A. Basile, P. E. Elia, and K. V. Holmes.** 1993. Mouse hepatitis virus strain A59 and blocking antireceptor monoclonal antibody bind to the N-terminal domain of cellular receptor. Proc. Natl. Acad. Sci. USA **90:**1716–1720.
24. **Enjuanes, L., I. Sola, F. Almazan, J. Ortego, A. Izeta, J. M. Gonzalez, S.**

Alonso, J. M. Sanchez, D. Escors, E. Calvo, C. Riquelme, and C. Sanchez. 2001. Coronavirus derived expression systems. J. Biotechnol. **88:**183–204.
25. **Gorbalenya, A. E., E. V. Koonin, A. P. Donchenko, and V. M. Blinov.** 1989. Coronavirus genome: prediction of putative functional domains in the nonstructural polyprotein by comparative amino acid sequence analysis. Nucleic Acids Res. **17:**4847–4861.
26. **Koetzner, C. A., M. M. Parker, C. S. Ricard, L. S. Sturman, and P. S. Masters.** 1992. Repair and mutagenesis of the genome of a deletion mutant of the coronavirus mouse hepatitis virus by targeted RNA recombination. J. Virol. **66:**1841–1848.
27. **Kuo, L., G.-J. Godeke, J. B. M. Raamsman, P. S. Masters, and P. J. M. Rottier.** 2000. Retargeting of coronavirus by substitution of the spike glycoprotein ectodomain: crossing the host cell species barrier. J. Virol. **74:**1393–1406.
28. **Kyuwa, S., and S. A. Stohlman.** 1990. Pathogenesis of a neurotropic murine coronavirus, strain JHM in the central nervous system of mice. Semin. Virol. **1:**273–280.
29. **Lai, M. M. C., and D. Cavanagh.** 1997. The molecular biology of coronaviruses. Adv. Virus Res. **48:**1–100.
30. **Leparc-Goffart, I., S. T. Hingley, M. M. Chua, X. Jiang, E. Lavi, and S. R. Weiss.** 1997. Altered pathogenesis of a mutant of the murine coronavirus MHV-A59 is associated with a Q159L amino acid substitution in the receptor binding region of the spike protein. Virology **239:**1–10.
31. **Lu, X.-T., A. C. Sims, and M. R. Denison.** 1998. Mouse hepatitis virus 3c-like protease cleaves a 22-kilodalton protein from the open reading frame 1a polyprotein in virus-infected cells and in vitro. J. Virol. **72:**2265–2271.
32. **Lu, Y., X. Lu, and M. R. Denison.** 1995. Identification and characterization of a serine-like proteinase of the murine coronavirus MHV-A59. J. Virol. **69:**3554–3559.
33. **Luytjes, W., P. J. Bredenbeek, J. Charite, B.A. van der Zeijst, M. C. Horzinek, and W. J. Spaan.** 1987. Primary structure of the glycoprotein E2 of coronavirus MHV-A59 and identification of the trypsin cleavage site. Virology **161:**479–487.
34. **Luytjes, W., P. J. Bredenbeek, A. F. Noten, M. C. Horzinek, and W. J. Spaan.** 1988. Sequence of mouse hepatitis virus A59 mRNA 2: indications for RNA recombination between coronaviruses and influenza C virus. Virology **166:** 415–422.
35. **Makino, S., J. G. Keck, S. A. Stohlman, and M. M. C. Lai.** 1986. High-frequency RNA recombination of murine coronaviruses. J. Virol. **57:**729–737.
36. **Murano, R., A. Wunderlich, A. Thor, J. Lundy, R. Noguchi, R. Cunningham, and J. Schlom.** 1985. Definition by monoclonal antibodies of a repertoire of epitopes on carcinoembryonic antigen differentially expressed in human colon carcinomas versus normal adult tissues. Cancer Res. **45:**5769–5780.
37. **Parker, M. M., and P. S. Masters.** 1990. Sequence comparison of the N genes of five strains of the coronavirus mouse hepatitis virus suggests a three-domain structure for the nucleocapsid protein. Virology **179:**463–468.
38. **Risco, C., I. M. Anton, L. Enjuanes, and J. L. Carrascosa.** 1996. The transmissible gastroenteritis coronavirus contains a spherical core shell consisting of M and N proteins. J. Virol. **70:**4773–4777.
39. **Sambrook, J., E. F. Fritsch, and T. Maniatis.** 1989. Molecular cloning: a laboratory manual, 2nd ed., p. 5.1–5.31. Cold Spring Harbor Laboratory Press, Cold Spring Harbor, N.Y.
40. **Schaad, M. C., and R. S. Baric.** 1994. Genetics of mouse hepatitis virus transcription: evidence that subgenomic negative strands are functional templates. J. Virol. **68:**8169–8179.
41. **Schickli, J. H., B. D. Zelus, D. E. Wentworth, S. G. Sawicki, and K. V. Holmes.** 1997. The murine coronavirus mouse hepatitis virus strain A59 from persistently infected murine cells exhibits an extended host range. J. Virol. **71:**9499–9507.
42. **Sethna, P. B., S.-L. Huang, and D. A. Brian.** 1989. Coronavirus subgenomic minus strand RNAs and the potential for mRNA replicons. Proc. Natl. Acad. Sci. USA **86:**5626–5630.
43. **Siddell, S. G.** 1995. The coronaviridae: an introduction, p. 1–10. *In* S. G. Siddell (ed.), The coronaviridae. Plenum Press, New York, N.Y.
44. **Sims, A. C., J. Ostermann, and M. R. Denison.** 2000. Mouse hepatitis virus replicase proteins associate with two distinct populations of intracellular membranes. J. Virol. **74:**5647–5654.
45. **Snijder, E. J., and M. C. Horzinek.** 1993. Toroviruses: replication, evolution and comparison with other members of the coronavirus-like superfamily. J. Gen. Virol. **74:**2305–2316.
46. **Stalcup, R. P., R. S. Baric, and J. L. Leibowitz.** 1998. Genetic complementation among three panels of mouse hepatitis virus gene 1 mutants. Virology **241:**112–121.
47. **Tahara, S. M., T. A. Dietlin, C. C. Bergmann, G. W. Nelson, S. Kyuwa, R. P. Anthony, and S. A. Stohlman.** 1994. Coronavirus translational regulation: leader effects mRNA efficiency. Virology **202:**621–630.
48. **Thiel, V., J. Herold, B. Schelle, and S. G. Siddell.** 2001. Infectious RNA transcribed in vitro from a cDNA copy of the human coronavirus genome cloned in vaccinia virus. J. Gen. Virol. **82:**1273–1281.
49. **Thiel, V., A. J. Herold, B. Schelle, and S. G. Siddell.** 2001. Viral replicase gene products suffice for coronavirus discontinuous transcription. J. Virol. **75:**6676–6681.
50. **Vennema, H., G. J. Godeke, J. W. A. Rossen, W. F. Voorhout, M. C. Horzinek, D. J. E. Opstelten, and P. J. M. Rottier.** 1996. Nucleocapsid-independent assembly of coronavirus-like particles by coexpression of viral envelope protein genes. EMBO J. **15:**2020–2028.
51. **Yokomori, K., S. A. Stohlman, and M. M. C. Lai.** 1993. The detection and characterization of multiple hemagglutinin-esterase (HE)-defective viruses in the mouse brain during subacute demyelination induced by mouse hepatitis virus. Virology **192:**170–178.
52. **Yount, B., K. M. Curtis, and R. S. Baric.** 2000. Strategy for systematic assembly of large RNA and DNA genomes: the transmissible gastroenteritis virus model. J. Virol. **74:**10600–10611.
53. **Yu, X., W. Bi, S. R. Weiss, and J. L. Leibowitz.** 1994. Mouse hepatitis gene 5b protein is a new virion envelope glycoprotein. Virology **202:**1018–1023.
54. **Zelus, B. D., D. R. Wessner, R. K. Williams, M. N. Pensiero, F. T. Phibbs, M. deSouza, G. S. Dveksler, and K. V. Holmes.** 1998. Purified, soluble recombinant mouse hepatitis virus receptor, $Bgp1^b$, and Bgp2 murine coronavirus receptors differ in mouse hepatitis virus binding and neutralizing activities. J. Virol. **72:**7237–7244.